https://doi.org/10.3311/PPch.39496

Periodica Polytechnica Chemical Engineering, 69(2), pp. 329–338, 2025

Investigation of the Structural, Thermal, Spectroscopic, and Electronic Properties of Praseodymium-based Hydroxyapatites Co-doped with Silver and Zinc in Varying Concentrations

Rebaz Obaid Kareem[1*], Tankut Ates[2], Azeez A. Barzinjy[3,4], Mehmet Mürşit Temüz[5], Turan İnce[6], Niyazi Bulut[6], Serhat Keser[7], Omer Kaygili[6]

[1] Department of Physics, College of Science, University of Halabja, 46018 Halabja, Iraq
[2] Department of Engineering Basic Sciences, Faculty of Engineering and Natural Sciences, Malatya Turgut Özal University, 44210 Battalgazi, Malatya, Türkiye
[3] Department of Physics, Faculty of Science, Soran University, 44008 Soran, Kurdistan Region, Iraq
[4] Department of Physics Education, Faculty of Education, Tishk International University, 44001 Erbil, Iraq
[5] Department of Chemistry, Faculty of Sciences, Firat University, 23119 Elazig, Türkiye
[6] Department of Physics, Faculty of Sciences, Firat University, 23119 Elazig, Türkiye
[7] Department of Chemistry and Chemical Processing Technology, Vocational School of Elazığ Organized Industrial Zone, Firat University, 23119, Elazig, Türkiye
[*] Corresponding author, e-mail: rebaz.katreem@uoh.edu.iq

Received: 05 December 2024, Accepted: 14 February 2025, Published online: 24 March 2025

Abstract

This study investigates the crystal structure, energy gap, band structure, spectroscopy, thermal, and electrical properties of Pr^{3+}-based hydroxyapatites (HAp) co-doped with Zn^{2+} and Ag^{+} in varying concentrations. The synthesized samples, designated as 0.25Zn-0.25Pr-HAp, 0.50Zn-0.25Pr-HAp, 0.75Zn-0.25Pr-HAp, 0.25Ag-0.25Pr-HAp, 0.50Ag-0.25Pr-HAp, and 0.75Ag-0.25Pr-HAp, were prepared using a wet chemical method. The materials were characterized by Fourier-transform infrared (FTIR) spectroscopy, X-ray diffraction (XRD), differential thermal analysis (DTA), and thermogravimetric analysis (TGA). Additionally, theoretical calculations employing density functional theory (DFT) were conducted to analyze the band structure (BS), energy gap (E_g; E_{HOMO}-E_{LUMO}), and density of states (DOS). Results revealed a progressive reduction in the bandgap with increasing dopant concentrations, particularly in Ag-doped samples. Notably, 0.75Ag-0.25Pr-HAp exhibited the smallest bandgap of 3.983 eV, indicating enhanced electronic conductivity and potential applications in bioelectronics and medical sensors. Furthermore, the co-doped samples demonstrated reduced crystallinity, larger crystallite sizes, and excellent stability in biological environments, alongside superior biocompatibility and antibacterial properties. Among the synthesized materials, 0.75Ag-0.25Pr-HAp exhibited promising characteristics as a biomedical material for bone-related applications, owing to its structural stability, enhanced electrical properties, and suitability in antibacterial and bioelectronic devices. This investigation highlights the versatility of Zn/Ag co-doped Pr-HAp materials for advanced biomedical and technological applications.

Keywords

hydroxyapatite, Zn/Ag co-doping, praseodymium-based hydroxyapatites, bandgap, wet chemical method

1 Introduction

Among the various inorganic components of the human body, calcium orthophosphates are particularly significant for forming essential structures such as bones, teeth, and antlers. Among these, hydroxyapatite (HAp) stands out as one of the most well-known bioceramic materials widely used in biomedicine. HAp is composed of calcium phosphate (CaP) and has many potential uses, including dental and orthopedic implants and prostheses [1, 2].

In addition to possessing several crucial qualities, HAp is essentially identical to the inorganic component that is found in bones and teeth structure. HAp is a highly versatile material ideal for applications involving

Cite this article as: Kareem, R. O., Ates, T., Barzinjy, A. A., Temüz, M. M., İnce, T., Bulut, N., Keser, S., Kaygili, O. "Investigation of the Structural, Thermal, Spectroscopic, and Electronic Properties of Praseodymium-based Hydroxyapatites Co-doped with Silver and Zinc in Varying Concentrations", Periodica Polytechnica Chemical Engineering, 69(2), pp. 329–338, 2025. https://doi.org/10.3311/PPch.39496

the regeneration and repair of hard tissues. Its exceptional biocompatibility, thermal stability, high bioactivity, and non-toxic nature make it a cornerstone in biomedical science [3, 4]. Additionally, HAp has the ability to exchange its ions with foreign ions, a property that can significantly improve its biocompatibility, mechanical properties, and microstructural characteristics. The most common calcium orthophosphates are HAp, and tricalcium phosphate (TCP), having the formula $Ca_3(PO_4)_2$ in two types of α and β phases [3, 5–7]. The chemical formula for HAp is $Ca_{10}(PO_4)_6(OH)_2$, and it has a Ca:P molar ratio of 1.67 [8]. The synthetic HAp may exist in two crystal structures: hexagonal or monoclinic [9, 10].

The use of HAp as an implant material in the medical industry is limited by its inherently weak mechanical properties. To address this challenge, various chemical dopants are incorporated into pure HAp to enhance its mechanical performance and make it more suitable for high-performance applications. Earlier experiments, and theoretical doped HAp with a variety of ions, including Mg^{2+}, Ni^{2+}, K^+, Ag^+, Na^+, Cu^{2+}, Co^{2+}, Sr^{2+}, Ba^{2+}, Zn^{2+}, Mg^{2+}, Pb^{2+}, Cd^{2+}, Y^{3+}, La^{3+}, Ce^+, Al^{3+}, CO_3^{2-}, F^-, Br^-, and Cl^- [9, 11–13]. All of these ions can interchange Ca^{2+}, PO_4^{3-}, and OH^- ions inside the crystalline lattice of HAp, which results in significant alterations to the material's mechanical and biological characteristics throughout the process. This results in a decrease in the Ca/P ratio, potentially enhancing solubility and influencing the crystal structure. Even small cationic substitutions can significantly impact the structural characteristics of HAp, including its crystal structure, lattice parameters, morphology, magnetic properties, thermal stability, and mechanical performance [8, 14].

The synthesis of HAp provides enhanced control over its material properties. Various methods have been employed for HAp synthesis, including sol-gel, hydrothermal, solid-state reactions, as well as dry and wet chemical techniques [8, 15]. Pr^{3+}, the third element in the lanthanide series with an atomic number of 59, is a rare earth element belonging to the light lanthanide group. It is not essential to functionally substitute calcium with Pr^{3+} ions to replace it in proteins and cell membranes. Lanthanide ions, including Pr^{3+}, exhibit biological properties similar to Ca^{2+} due to their comparable ionic radii [16, 17]. For a long time, Ag^+ was used as a disinfectant. It possesses a wide range of antibacterial properties and exhibits low toxicity to mammals. In other words, the combination of HAp and Ag nanoparticles demonstrates exceptional antibacterial properties, making it an ideal biomaterial for treating bacterial bone infections such as osteomyelitis. This is particularly crucial for addressing the diverse types of bacteria that can colonize biomaterials and lead to infections [18, 19]. Recent studies suggest that small quantities of silver exhibit antibacterial properties, whereas higher concentrations can be toxic [20]. Zn^{2+} plays a vital role in regulating enzyme activity and aids in the absorption and release of minerals from the bone reservoir in the body [21]. Multiple studies have developed Zn-doped HAps for use as antibacterial agents [22, 23]. Examples include applications in bone grafting, coatings on metallic implants to enhance biocompatibility and biological activity and promoting bone mineralization [24].

In our previous research by Sahin et al. [25] different concentrations of Zn/Ag co-doped HAp based on praseodymium were synthesized, including five distinct compositions: 0.4Pr-HAp, 0.4Zn-0.4Pr-HAp, 0.8Zn-0.4Pr-HAp, 0.4Ag-0.4Pr-HAp, and 0.8Zn-0.4Pr-HAp. These samples were analyzed using density of states (DOS) and band structure (BS) calculations. The band gap values ranged from 4.4037 eV to 4.1554 eV, indicating a reduction in energy from 0.4Pr-HAp to 0.8Ag-0.4Pr-HAp. Theoretical studies revealed a consistent decrease in the band gap with the addition of Ag or Zn co-dopants in Pr-based HAp. The discoveries by Sahin et al. [25] significantly impact the tunability of the electrical properties of HAp through controlled doping with Zn, Pr, and Ag. Enhancing these favorable electronic properties is crucial for applications such as coatings for biocompatible electronics and other related fields. The study by Sinulingga et al. [26] demonstrates that the 2.5Ag/2.5Zn co-doping approach in HAp can enhance osteoblastic cell proliferation and improve antibacterial activity. This co-doping method was found to be significantly more effective compared to 2.5Ag-doped HAp or 5Ag-doped HAp.

In the current investigation, six different concentrations of Zn/Ag co-doped HAp based on Pr were synthesized using a wet chemical process, which is a facile method for preparing nanomaterials having high purity. The samples were designated as 0.25Zn-0.25Pr-HAp, 0.50Zn-0.25Pr-HAp, 0.75Zn-0.25Pr-HAp, 0.25Ag-0.25Pr-HAp, 0.50Ag-0.25Pr-HAp, and 0.75Ag-0.25Pr-HAp. A series of experimental evaluations, including X-ray diffraction (XRD), Fourier-transform infrared (FTIR) spectroscopy, differential thermal analysis (DTA), and thermogravimetric analysis (TGA), were conducted on the samples. Additionally, theoretical calculations using density functional theory (DFT) were performed to investigate the BS, energy gap E_g, and DOS.

2 Materials and method

(49.875 − x) mmol calcium nitrate tetrahydrate (Carlo Erba), 0.125 mmol praseodymium (III) nitrate hexahydrate (Alfa Aesar), x mmol zinc acetate dihydrate (Carlo Erba) were dissolved in distilled water for the Zn-doped samples. Instead of the zinc acetate dehydrate, x mmol silver nitrate (Sigma-Aldrich) was used to prepare the Ag-doped samples. Here x was selected as 0.125, 0.250 and 0.375, respectively. 30.0 mmol diammonium hydrogen phosphate (Merck) was dissolved in the same solvent and added drop wisely to the first mixture. For all the samples, the pH of the final solution was adjusted to 10.0 using ammonia solution (Sigma-Aldrich) and all the mixtures were stirred at 65 °C for 4 h. After stirring these were dried in an oven at 120 °C for 38 h, and the as-dried powders were calcined in an electric furnace at 900 °C for 3 h. The preparation of the 0.25Zn-0.25Pr-HAp, 0.50Zn-0.25Pr-HAp, 0.75Zn-0.25Pr-HAp, 0.25Ag-0.25Pr-HAp, 0.50Ag-0.25Pr-HAp, and 0.75Ag-0.25Pr-HAp samples was carried out, where these numbers point out the atomic percentage of each dopant in the HAp structure.

XRD data were collected using a Bruker D8 Advance diffractometer with Cu-Kα radiation. FTIR measurements were conducted using a PerkinElmer Spectrum One spectrophotometer with KBr pellets. A Perkin Elmer Diamond TG/DTA was used to record DTA and TGA data.

3 Results and discussion

3.1 XRD analysis

As shown in Fig. 1, the XRD patterns of the HAps in their as-prepared state are presented. The primary phase identified was HAp (JCPDS 09-0432), while the secondary phase was β-TCP (JCPDS 09-0169). A comparison is made between the theoretical and experimental XRD values, obtained after optimization, with the lattice parameters (a and c) and unit cell volume (V) of these samples, which are summarized in Table 1.

Equation (1) was used to calculate the a and c lattice parameters [27]:

$$\frac{1}{d^2} = \frac{4}{3}\left(\frac{h^2 + hk + k^2}{a^2}\right) + \frac{l^2}{c^2}. \tag{1}$$

Where h, k and l are Miller indices and d is the interplanar distance.

To calculate the volume of unit cells V (nm^3) of the hexagonal unit cell, Eq. (2) was utilized, which is expressed as follows:

$$V = 0.866a^2c. \tag{2}$$

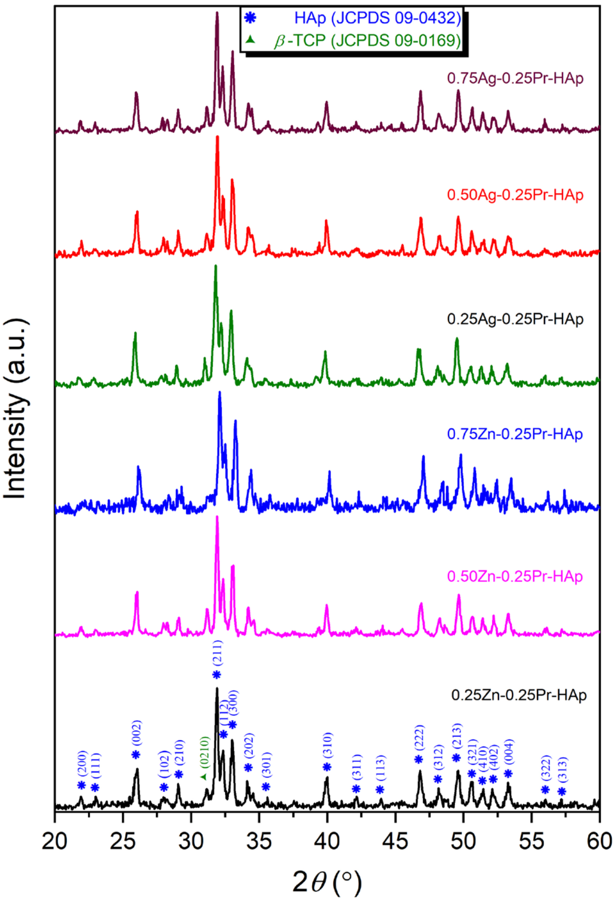

Fig. 1 The XRD patterns of Zn or Ag co-doped HAp based Pr-HAp samples

According to the findings of a recent study, the XRD lattice parameters for pure HAp were found to be in agreement with the following values: $a = b$ and c are 0.9418 nm and 0.6884 nm, respectively, and V = 0.5288 nm^3 also exists [28].

A relationship exists between the percentage of crystallinity, denoted as X_C%, and the solubility of the Zn/Ag co-doped HAp based Pr concentrations. Equation (3) was used to determine the X_C% for each sample. This was accomplished by using the intensity (I_{300}) of the (300) reflection in conjunction with the intensity of the pit ($V_{112/300}$) that existed concurrently between the (112) and (300) reflections.

$$X_C\% = \left(1 - \frac{V_{112/300}}{I_{300}}\right) \times 100 \tag{3}$$

For the purpose of determining the size D of the crystallites, the Scherer formula was used [29]:

$$D = \frac{0.9\lambda}{\beta\cos\theta}. \tag{4}$$

Table 1 Comparison of theoretical and experimental XRD results

Sample code	Theoretical			Experimental				
	a (nm)	*c* (nm)	*V* (nm^3)	*a* (nm)	*c* (nm)	*V* (nm^3)	X_C (%)	*D* (nm)
0.25Zn-0.25Pr-HAp	0.9489	0.6795	0.5298	0.9395	0.6848	0.5235	84.74	29.76
0.50Zn-0.25Pr-HAp	0.9487	0.6802	0.5302	0.9381	0.6834	0.5208	90.17	28.89
0.75Zn-0.25Pr-HAp	0.9471	0.6810	0.5290	0.9326	0.6797	0.5120	87.04	28.67
0.25Ag-0.25Pr-HAp	0.9418	0.6808	0.5229	0.9384	0.6833	0.5211	85.62	29.75
0.50Ag-0.25Pr-HAp	0.9418	0.6880	0.5285	0.9387	0.6863	0.5237	90.00	32.35
0.75Ag-0.25Pr-HAp	0.9460	0.6884	0.5335	0.9411	0.6879	0.5276	91.58	31.24

Table 1 shows the XRD related data of the Zn or Ag co-doped Pr based HAp samples with the sample codes: 0.25Zn-0.25Pr-HAp, 0.50Zn-0.25Pr-HAp, 0.75Zn-0.25Pr-HAp, 0.25Ag-0.25Pr-HAp, 0.50Ag-0.25Pr-HAp, and 0.75Ag-0.25Pr-HAp. The numbers indicate the atomic percentage (at%) of each dopant in the HAp structure.

The experimental and theoretical values of the *a* and *c* lattice parameters, as well as the unit cell volume, were influenced by the quantity and type of Zn or Ag in the co-doped Pr based HAp samples. Theoretical values indicate an increase in both the *a* and *c* lattice parameters for all samples, except for 0.25Zn-0.25Pr-HAp, 0.50Zn-0.25Pr-HAp, and 0.75Zn-0.25Pr-HAp. Similarly, *V* increased for all samples, except for the 0.75Zn-0.25Pr-HAp sample (Table 1). In the experimental investigations, the *a* and *c* lattice parameters, as well as the unit cell volume, decreased with increasing Zn co-doping concentrations in Pr-based HAp. For Zn-doped samples, these parameters decreased with 0.25 at% Zn addition but increased with 0.75 at% Zn addition at 0.25% Pr concentration (Table 1). Since Zn^{2+} (0.074 nm) has a smaller ionic radius than Ca^{2+} (0.099 nm), it may reduce the lattice parameters *a* and *c*, as well as the unit cell volume. Also, the HAp structural stability may improve with this modification by Zn ions. Our findings suggest that the theoretical and experimental values are in close agreement, with only minor discrepancies. This indicates that the samples with the lowest Zn content, i.e., the 0.25Zn-0.25Pr-HAp sample, exhibited the smallest crystallinity, the largest crystallite size, and the smallest unit cell volume. In contrast, the largest *V* and crystallinity were observed in the sample with the highest Ag content (0.75 at% Ag) (Fig. 1). Crystallinity of HAp samples affects their solubility and biological characteristics. Low solubility correlates with high crystallinity. Solubility, like crystallinity, impacts crystal size [30, 31]. Fig. 2 illustrates the experimental and theoretical relationship between *V* and the lattice parameters *a* and *c*.

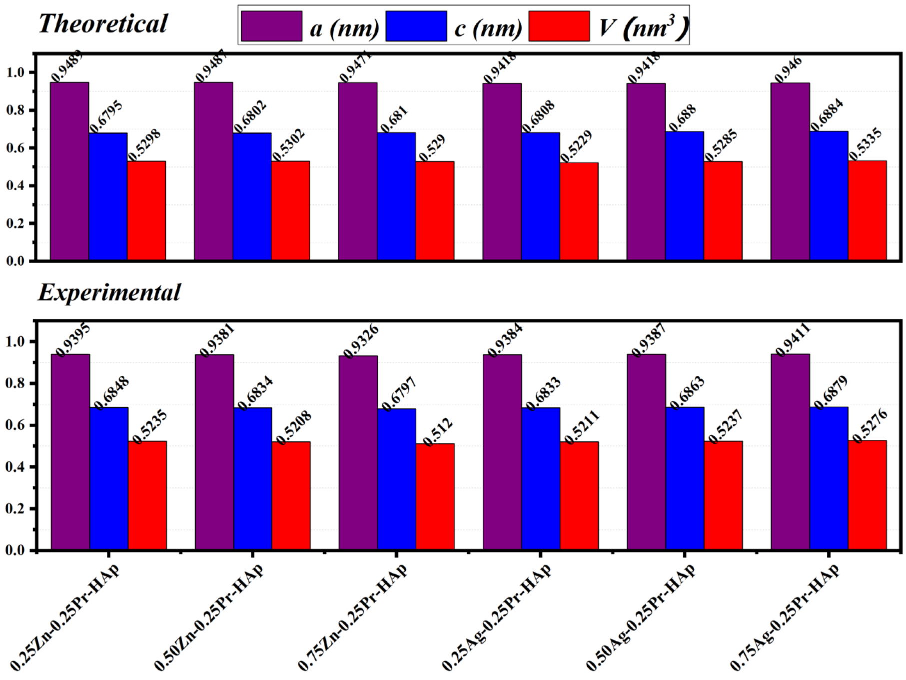

Fig. 2 The theoretical and experimental values of *a*, *c* and *V*

Based on our recent research by Sahin et al. [25], the 0.8% Zn or Ag co-doped Pr^{3+} based HAp was characterized by smaller crystallinity and larger crystallite size. In comparison, our current study shows that this material holds promise for various biomedical application, including bone-related treatments and implants, due to its antibacterial properties, stability in biological settings, and biocompatibility. The observed reduction in crystallinity strongly suggests that the Pr, Zn, and Ag ions have been successfully incorporated into the HAp samples.

3.2 FTIR spectroscopy analysis

FTIR spectroscopy was employed to identify and analyze specific functional groups. The wave numbers associated with the Zn or Ag co-doped Pr based HAp ranged from 400 to 4000 cm^{-1} (Fig. 3). The bands of PO_4^{-3} group were recorded at 553 (υ_2), 597 (υ_4), 960 (υ_1), 1020 (υ_3), and 1089 (υ_3) cm^{-1} in the FTIR spectra. As a result of this investigation, the vibrational modes of the OH^- group are connected to the bands that were detected at 629, and 3570 cm^{-1}, respectively (Fig. 3). Lastly, our findings concurred with

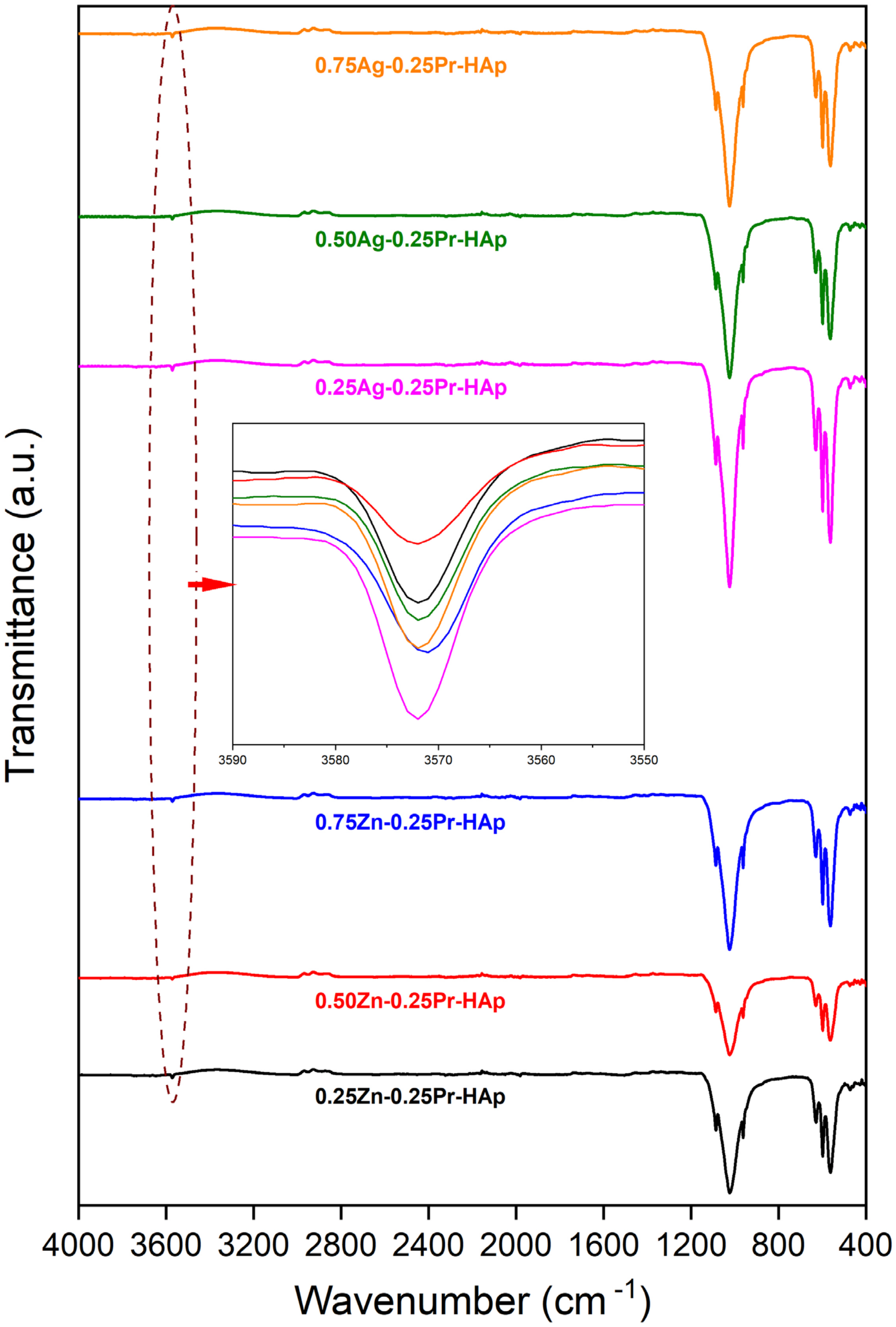

Fig. 3 The as-plotted FTIR investigations of the Zn or Ag co-doped Pr-based HAp

Zn or Ag co-doped Pr based HAp [25], Ag-HAp [18], Zn-HAp [21], and Pr-HAp [17].

3.3 Thermal characterization

DTA is a thermal analysis technique used to measure the temperature difference between a sample and an inert reference material as they undergo the same heating or cooling process [32]. DTA thermograms of the HAp samples in their as-produced state are shown in Fig. 4.

There is no peak associated with phase change for the Zn or Ag co-doped Pr-based HAp samples. These results are in excellent agreement with the literature [17, 27], since all the samples that were created in their original state are thermally stable in the temperature range of ambient 25 to 1000 °C.

TGA measures changes in a sample mass during heating or cooling, through tracking mass variations with temperature, TGA evaluates the thermal stability and composition of the material [33]. The mass losses were detected as 1.26%, 0.33%, 0.38%, 1.00%, 0.26% and 1.45% for the samples of 0.25Zn-0.25Pr-HAp, 0.50Zn-0.25Pr-HAp, 0.75Zn-0.25Pr-HAp, 0.25Ag-0.25Pr-HAp, 0.50Ag-0.25Pr-HAp, and 0.75Ag-0.25Pr-HAp, respectively (Fig. 5). According to the prior study by Sahin et al. [25], the TGA and DTA results showed that the as-used Zn or Ag co-dopants in the Pr-based HAp did not affect the thermal properties of the samples.

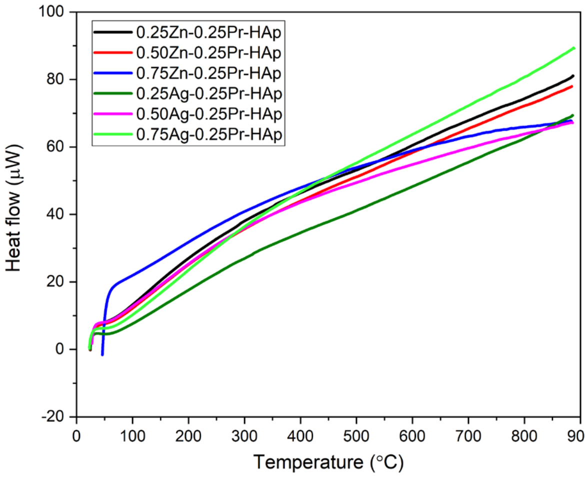

Fig. 4 The DTA results for the HAp samples

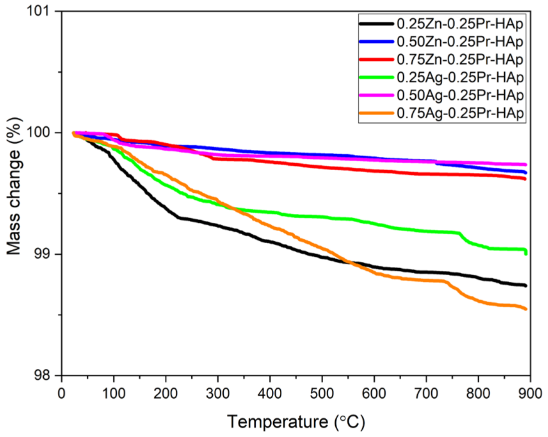

Fig. 5 The TGA results for the HAp samples

3.4 Theoretical computations

During the theoretical investigations, the BS, DOS, and E_g calculations were performed using DFT. All the simulated theoretical findings were obtained using the CASTEP Software [15, 34]. The Dirac δ-function expression describes the DOS with specified energy [8, 34, 35]:

$$\mathrm{DOS}(E) = 2\sum \delta\left(E - \varepsilon_i\right). \tag{5}$$

In Eq. (5), δ is a Dirac function, E is representing the total energy, and ε_i is the energy of the i^{th} molecular orbital. The factor of two is used to count spins that are degenerate. The estimated DOS, BS, and energy gap for every synthesized Pr-based HAp co-doped with Zn/Ag at different percentages, with sample names: specifically, 0.25Zn-0.25Pr-HAp, 0.50Zn-0.25Pr-HAp, 0.75Zn-0.25Pr-HAp, 0.25Ag-0.25Pr-HAp, 0.50Ag-0.25Pr-HAp, and 0.75Ag-0.25Pr-HAp samples.

3.4.1 BS and DOS calculations

In quantum mechanical systems, modern DFT algorithms can calculate a wide range of phenomena, including electronic structure, chemical and optical properties, band structures, spectroscopic features, elastic and vibrational properties, crystal structures, and thermal characteristics. Moreover, the capacity to predict how theoretical and experimental findings relate to structure and properties [36–38]. The electronic DOS quantifies how "packed" the electrons are in energy levels in addition to referring to the quantity of accessible quantum states per energy unit. A high DOS at a given energy level indicates that multiple states are available for occupation, influencing both electrical conductivity and heat capacity [15].

The electronic band gap of a material is defined as the difference between its electron affinity—the energy required to add an electron to the structure—and its first ionization energy—the energy needed to remove an electron from the system. Both energies can be calculated using conventional DFT, forming the basis of the delta-SCF method, a technique for determining band gap properties [39, 40]. The band gaps were measured and acquired at intervals ranging from G to H. The BS calculations and DOS findings for a Pr-based HAp with Zn or Ag at different percentages: 0.25, 0.50, and 0.75 at% are shown in Fig. 6.

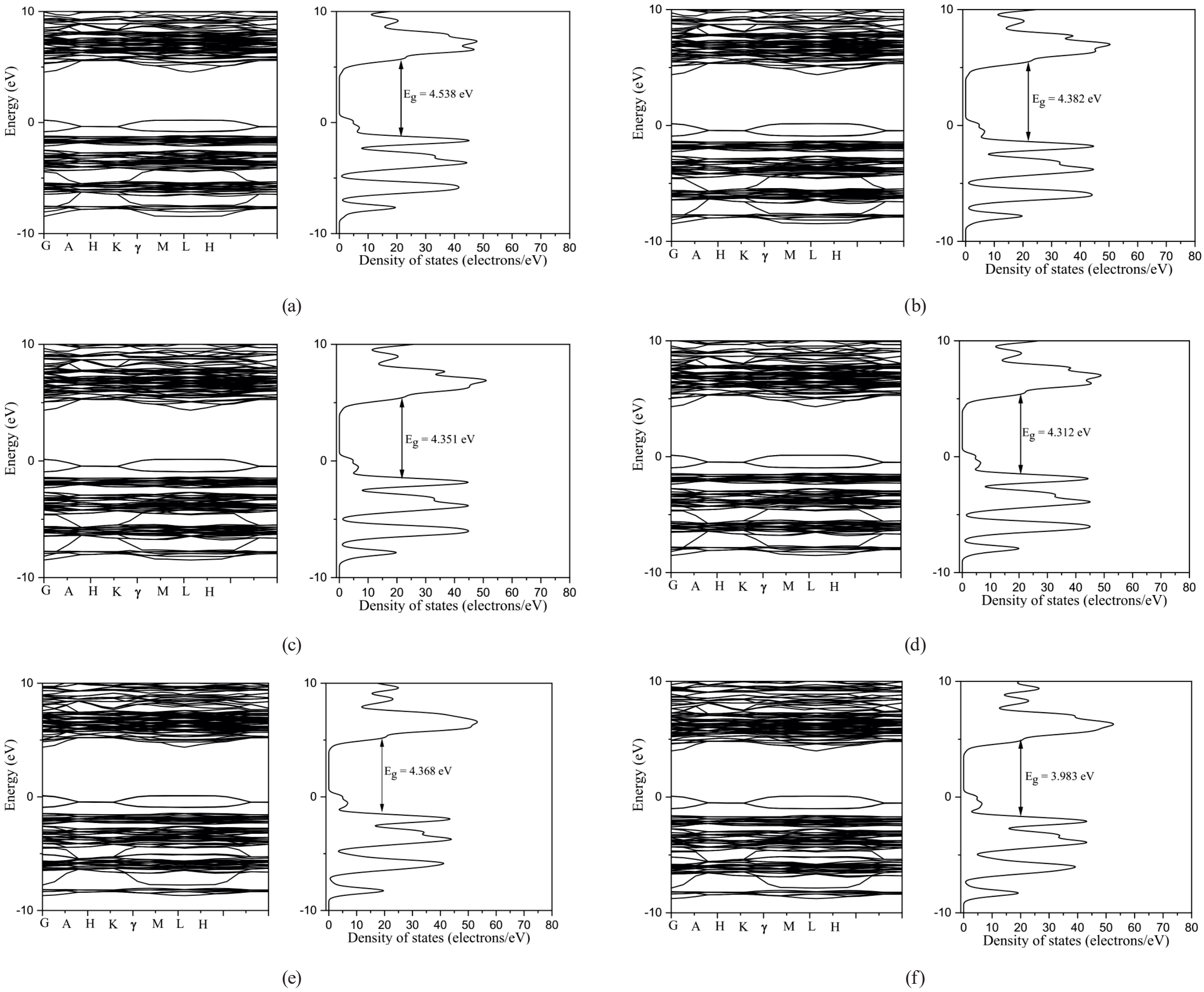

Fig. 6 Band structure, and density of states calculations of Zn^{2+} or Ag^{+} co-doped Pr^{3+} based HAp samples: (a) 0.25Zn-0.25Pr-HAp, (b) 0.50Zn-0.25Pr-HAp, (c) 0.75Zn-0.25Pr-HAp, (d) 0.25Ag-0.25Pr-HAp, (e) 0.50Ag-0.25Pr-HAp, and (f) 0.75Ag-0.25Pr-HAp

The electronic properties of HAp doped with 0.25% Pr and co-doped with varying concentrations of Zn or Ag were systematically investigated to evaluate the impact of dopant composition on the band gap and DOS as shown in Fig. 6. The studied compositions include 0.25Zn-0.25Pr-HAp, 0.50Zn-0.25Pr-HAp, 0.75Zn-0.25Pr-HAp, 0.25Ag-0.25Pr-HAp, 0.50Ag-0.25Pr-HAp, and 0.75Ag-0.25Pr-HAp, with corresponding band gap values of 4.538 eV, 4.382 eV, 4.351 eV, 4.312 eV, 4.368 eV, and 3.983 eV, respectively. The gradual reduction in band gap with increasing dopant concentration, particularly in Ag-doped systems, suggests a notable improvement in electronic conductivity. Exploring the small band gaps in Ag-doped HAp could uncover enhanced electrical properties, making them suitable for applications in bioelectronics or medical sensors. Notably, the 0.75Ag-0.25Pr-HAp composition exhibits the smallest band gap of 3.983 eV. Sinulingga et al. [26] concluded that using the 2.5%Ag/2.5%Zn co-doped HAp biomaterials were extremely more effective than 2.5%Ag-doped HAp or 5%Ag-doped HAp. This trend can be attributed to the ability of Zn and Ag co-dopants to introduce localized electronic states within the band gap, thereby altering the electronic structure of the HAp matrix.

The discoveries of Sahin et al. [25] on the Zn or Ag co-dopants Pr-based HAp, and our current investigation revealed that the Ag concentration may increase HAp's structural stability, corrosion efficiency, reactivity, safety *in vivo*, as well as improve bioactivity. [26]. These modifications suggest that the co-dopants not only reduce the band gap but also enhance the electronic environment, making the material more conducive to electron transport.

Such tunability in electronic properties underscores the potential of Pr-, Zn-, and Ag-doped HAp as a multifunctional material suitable for a wide range of applications, including catalysis, biosensing, and electronic devices. The systematic variation in band gap energy and the associated changes in the DOS offer valuable insights for designing HAp-based materials with customized functionalities, expanding their potential applications in technological and biomedical fields.

4 Conclusions

This study investigates the crystal structure, spectroscopic, thermal, and electrical properties of Zn^{2+} and Ag^{+} co-doped Pr^{3+}-doped hydroxyapatites. Zn or Ag co-doped Pr-based HAp samples with varying concentrations were synthesized via wet chemical methods and analyzed using FTIR, XRD, DTA, and TGA. Theoretical calculations, including DFT, were employed to examine the BS, E_g, and DOS. DTA analysis revealed no phase change peaks for the Zn or Ag co-doped Pr-based HAp samples, and all samples were thermally stable within the temperature range of 25 to 1000 °C. The small band gaps in Ag-doped HAp suggests enhanced electrical characteristics, making them suitable for bioelectronics or medical sensors, 0.75Ag-0.25Pr-HAp exhibiting the smallest band gap of 3.983 eV. The progressive reduction in band gap with increasing dopant concentration, particularly in Ag-doped systems, highlights a notable improvement in electronic conductivity and corrosion efficiency, further supporting their potential applications in bioelectronics and medical sensors.

Acknowledgement

This work was supported by the Management Unit of Scientific Research Projects of Firat University, Turkey (FUBAP) (Project Numbers: FF.24.03, FF.24.22 and ADEP.24.09).

References

[1] Ghosh, R., Sarkar, R. "Synthesis and characterization of sintered hydroxyapatite: a comparative study on the effect of preparation route", Journal of the Australian Ceramic Society, 54(1), pp. 71–80, 2018. https://doi.org/10.1007/s41779-017-0128-5

[2] Dorozhkin, S. V. "Calcium orthophosphates: Occurrence, properties, biomineralization, pathological calcification and biomimetic applications", Biomatter, 1(2), pp. 121–164, 2011. https://doi.org/10.4161/biom.18790

[3] Kareem, R. O., Bulut, N., Kaygili, O. "Hydroxyapatite biomaterials: A comprehensive review of their properties, structures, medical applications, and fabrication methods", Journal of Chemical Reviews, 6(1), pp. 1–26, 2024. https://doi.org/10.48309/JCR.2024.415051.1253

[4] Sadat-Shojai, M., Khorasani, M.-T., Dinpanah-Khoshdargi, E., Jamshidi, A. "Synthesis methods for nanosized hydroxyapatite with diverse structures", Acta Biomaterialia, 9(8), pp. 7591–7621, 2013. https://doi.org/10.1016/j.actbio.2013.04.012

[5] Agrawal, K., Singh, G., Puri, D., Prakash, S. "Synthesis and characterization of hydroxyapatite powder by sol-gel method for biomedical application", Journal of Minerals & Materials Characterization & Engineering, 10(8), pp. 727–734, 2011. https://doi.org/10.4236/jmmce.2011.108057

[6] Williams, D. F. "The Williams Dictionary of Biomaterials", Liverpool University Press, 1999. ISBN 9780853239215

[7] Chen, Q., Thouas, G. "Biomaterials: A basic introduction", CRC Press, 2014. ISBN 9781482227697

[8] Korkmaz, A. A., Ahmed, L. O., Kareem, R. O., Kebiroglu, H., Ates, T., Bulut, N., Kaygili, O., Ates, B. "Theoretical and experimental characterization of Sn-based hydroxyapatites doped with Bi", Journal of the Australian Ceramic Society, 58(3), pp. 803–815, 2022. https://doi.org/10.1007/s41779-022-00730-5

[9] Bulut, N., Kaygili, O., Hssain, A. H., Dorozhkin, S. V., Abdelghani, B., Orek, C., Kebiroglu, H., Ates, T., Kareem, R. O. "Mg-Dopant Effects on Band Structures of Zn-Based Hydroxyapatites: A Theoretical Study", Iranian Journal of Science, 47(5), pp. 1843–1859, 2023. https://doi.org/10.1007/s40995-023-01531-6

[10] Mohammed, B. A., Ateş, T., Mahmood, B. K., Obaıd Kareem, R., Keser, S., Bulut, N., Kaygılı, O. "Investigation of the effects of glycerol addition as a catalyst on the morphology and structural properties of Gd/Er co-doped hydroxyapatite", Journal of Physical Chemistry and Functional Materials, 7(1), pp. 28–31, 2024. https://doi.org/10.54565/jphcfum.1458970

[11] Kaygili, O., Keser, S., Ates, T., Al-Ghamdi, A. A., Yakuphanoglu, F. "Controlling of dielectrical and optical properties of hydroxyapatite based bioceramics by Cd content", Powder Technology, 245, pp. 1–6, 2013. https://doi.org/10.1016/j.powtec.2013.04.012

[12] Aronov, D., Chaikina, M., Haddad, J., Karlov, A., Mezinskis, G., Oster, L., Pavlovska, I., Rosenman, G. "Electronic states spectroscopy of Hydroxyapatite ceramics", Journal of Materials Science: Materials in Medicine, 18(5), pp. 865–870, 2007. https://doi.org/10.1007/s10856-006-0080-3

[13] Kanchana, P., Sekar, C. "Influence of sodium fluoride on the synthesis of hydroxyapatite by gel method", Journal of Crystal Growth, 312(6), pp. 808–816, 2010. https://doi.org/10.1016/j.jcrysgro.2009.12.032

[14] Othmani, M., Bachoua, H., Ghandour, Y., Aissa, A., Debbabi, M. "Synthesis, characterization and catalytic properties of copper-substituted hydroxyapatite nanocrystals", Materials Research Bulletin, 97, pp. 560–566, 2018. https://doi.org/10.1016/j.materresbull.2017.09.056

[15] Kareem, R. O., Kaygili, O., Ates, T., Bulut, N., Koytepe, S., Kuruçay, A., Ercan, F., Ercan, I. "Experimental and theoretical characterization of Bi-based hydroxyapatites doped with Ce", Ceramics International, 48(22), pp. 33440–33454, 2022. https://doi.org/10.1016/j.ceramint.2022.07.287

[16] Zamani, H. A., Arvinfar, A., Rahimi, F., Imani, A., Ganjali, M. R., Meghdadi, S. "Praseodymium analysis in aqueous solution by Pr^{3+}–PVC membrane sensor based on *N*,*N*′-bis (4-hydroxysalicylidene)-1-3-phenylenediamine", Materials Science and Engineering: C, 31(2), pp. 307–312, 2011. https://doi.org/10.1016/j.msec.2010.09.016

[17] Agid, R. S., Kaygili, O., Bulut, N., Dorozhkin, S. V., Ates, T., Koytepe, S., Ates, B., Ercan, I., İnce, T., Mahmood, B. K. "Investigation of the effects of Pr doping on the structural properties of hydroxyapatite: an experimental and theoretical study", Journal of the Australian Ceramic Society, 56(4), pp. 1501–1513, 2020. https://doi.org/10.1007/s41779-020-00495-9

[18] Kim, H., Mondal, S., Jang, B., Manivasagan, P., Moorthy, M. S., Oh, J. "Biomimetic synthesis of metal–hydroxyapatite (Au-HAp, Ag-HAp, Au-Ag-HAp): Structural analysis, spectroscopic characterization and biomedical application", Ceramics International, 44(16), pp. 20490–20500, 2018. https://doi.org/10.1016/j.ceramint.2018.08.045

[19] Yang, H., Xiao, B., Xu, K.-W. "Synthesis and characterization of Ag/Cu/HAP with platelet morphology", Journal of Materials Science: Materials in Medicine, 20(3), pp. 785–792, 2009. https://doi.org/10.1007/s10856-008-3630-z

[20] Ciobanu, C. S., Massuyeau, F., Constantin, L. V., Predoi, D. "Structural and physical properties of antibacterial Ag-doped nano-hydroxyapatite synthesized at 100 °C", Nanoscale Research Letters, 6(1), 613, 2011. https://doi.org/10.1186/1556-276X-6-613

[21] Ofudje, E. A., Adeogun, A. I., Idowu, M. A., Kareem, S. O. "Synthesis and characterization of Zn-Doped hydroxyapatite: scaffold application, antibacterial and bioactivity studies", Heliyon, 5(5), e01716, 2019. https://doi.org/10.1016/j.heliyon.2019.e01716

[22] Thian, E. S., Konishi, T., Kawanobe, Y., Lim, P. N., Choong, C., Ho, B., Aizawa, M. "Zinc-substituted hydroxyapatite: a biomaterial with enhanced bioactivity and antibacterial properties", Journal of Materials Science: Materials in Medicine, 24(2), pp. 437–445, 2013. https://doi.org/10.1007/s10856-012-4817-x

[23] Ng, Y. H., Leung, Y. H., Liu, F. Z., Ng, A. M. C., Gao, M. H., Chan, C. M. N., Djurišić, A. B., Leung, F. C. C., Chan, W. K. "Antibacterial activity of ZnO nanoparticles under ambient illumination — The effect of nanoparticle properties", Thin Solid Films, 542, pp. 368–372, 2013. https://doi.org/10.1016/j.tsf.2013.05.167

[24] Chen, F., Wang, M., Wang, J., Chen, X., Li, X., Xiao, Y., Zhang, X. "Effects of hydroxyapatite surface nano/micro-structure on osteoclast formation and activity", Journal of Materials Chemistry B, 7(47), pp. 7574–7587, 2019. https://doi.org/10.1039/C9TB01204D

[25] Sahin, B., Ates, T., Acari, I. K., Barzinjy, A. A., Ates, B., Özcan, İ., Bulut, N., Keser, S., Kaygili, O. "Tuning electronic properties of hydroxyapatite through controlled doping using zinc, silver, and praseodymium: A density of states and experimental study", Ceramics International, 50(5), pp. 7919–7929, 2024. https://doi.org/10.1016/j.ceramint.2023.12.120

[26] Sinulingga, K., Sirait, M., Siregar, N., Doloksaribu, M. E. "Investigation of antibacterial activity and cell viability of Ag/Mg and Ag/Zn co-doped hydroxyapatite derived from natural limestone", ACS Omega, 6(49), pp. 34185–34191, 2021. https://doi.org/10.1021/acsomega.1c05921

[27] Keser, S., Dogan, A., Ates, T., Barzinjy, A. A., Ates, B., Tekin, S., Sandal, S., Kareem, R. O., Özcan, İ., Bulut, N. "Effects of gallic acid and quercetin on the structural, thermal, spectroscopic, *in vitro* biocompatibility and electronic properties of Au-based hydroxyapatite structure", Materials Chemistry and Physics, 327, 129892, 2024. https://doi.org/10.1016/j.matchemphys.2024.129892

[28] Paduraru, A. V., Musuc, A. M., Oprea, O. C., Trusca, R., Iordache, F., Vasile, B. S., Andronescu, E. "Synthesis and characterization of photoluminescent Ce(III) and Ce(IV) substituted hydroxyapatite nanomaterials by co-precipitation method: Cytotoxicity and biocompatibility evaluation", Nanomaterials, 11(8), 1911, 2021. https://doi.org/10.3390/nano11081911

[29] Acar, S., Kaygili, O., Ates, T., Dorozhkin, S. V., Bulut, N., Ates, B., Koytepe, S., Ercan, F., Kebiroglu, H., Hssain, A. H. "Experimental characterization and theoretical investigation of Ce/Yb co-doped hydroxyapatites", Materials Chemistry and Physics, 276, 125444, 2022. https://doi.org/10.1016/j.matchemphys.2021.125444

[30] Kareem, R. O. "Synthesis and Characterization of Bismuth-Based Hydroxyapatites Doped with Cerium", MSc Thesis, Firat University, Graduate School of Natural and Applied Sciences, 2023.

[31] Hssain, A. H., Bulut, N., Ates, T., Koytepe, S., Kuruçay, A., Kebiroglu, H., Kaygili, O. "Sr/Smco-doped hydroxyapatites: experimental characterization and theoretical research", Journal of the Australian Ceramic Society, 58(5), pp. 1491–1507, 2022. https://doi.org/10.1007/s41779-022-00788-1

[32] Watson, E. S., O'Neill, M. J., Justin, J., Brenner, N. "A Differential Scanning Calorimeter for Quantitative Differential Thermal Analysis", Analytical Chemistry, 36(7), pp. 1233–1238, 1964. https://doi.org/10.1021/ac60213a019

[33] Bottom, R. "Thermogravimetric analysis", In: Gabbott, P. (ed.) Principles and applications of thermal analysis, Wiley, 2008, pp. 87–118. ISBN 9780470697702 https://doi.org/10.1002/9780470697702.ch3

[34] Kaygili, O., Ercan, I., Ates, T., Keser, S., Orek, C., Gunduz, B., Seckin, T., Bulut, N., Bañares, L. "An experimental and theoretical investigation of the structure of synthesized ZnO powder", Chemical Physics, 513, pp. 273–279, 2018. https://doi.org/10.1016/j.chemphys.2018.08.021

[35] Hssain, A. H., Bulut, N., Ates, T., Koytepe, S., Kuruçay, A., Kebiroglu, H., Kaygili, O. "Experimental characterization and theoretical investigation of Zn/Sm co-doped hydroxyapatites", Materials Today Communications, 31, 103850, 2022. https://doi.org/10.1016/j.mtcomm.2022.103850

[36] Hasnip, P. J., Refson, K., Probert, M. I. J., Yates, J. R., Clark, S. J., Pickard, C. J. "Density functional theory in the solid state", Philosophical Transactions of the Royal Society A: Mathematical, Physical and Engineering Sciences, 372(2011), 20130270, 2014.
https://doi.org/10.1098/rsta.2013.0270

[37] Tanış, E. "New optoelectronic material based on biguanide for orange and yellow organic light emitting diode: A combined experimental and theoretical study", Journal of Molecular Liquids, 358, 119161, 2022.
https://doi.org/10.1016/j.molliq.2022.119161

[38] Tanış, E. "Optical and photonic properties dependence on HNMB solvents: An emitter molecule for OLEDs", Optik, 252, 168576, 2022.
https://doi.org/10.1016/j.ijleo.2022.168576

[39] Perdew, J. P., Parr, R. G., Levy, M., Balduz Jr, J. L. "Density-functional theory for fractional particle number: Derivative discontinuities of the energy", Physical Review Letters, 49(23), pp. 1691–1694, 1982.
https://doi.org/10.1103/PhysRevLett.49.1691

[40] Tanış, E. "Study of electronic, optoelectronic and photonic properties of NBB material in solvent environments", Journal of Electronic Materials, 51(9), pp. 4978–4985, 2022.
https://doi.org/10.1007/s11664-022-09730-4